sustainability

MDPI

Article

Numerical Simulation Study on the Effects of Co-Injection of Pulverized Coal and Hydrochar into the Blast Furnace

Tao Li [1,2], Guangwei Wang [1,2,*], Heng Zhou [1,2], Xiaojun Ning [1,2] and Cuiliu Zhang [2]

[1] State Key Laboratory of Advanced Metallurgy, University of Science and Technology Beijing, Beijing 100083, China; honortao666@gmail.com (T.L.); zhouheng@ustb.edu.cn (H.Z.); ningxj@ustb.edu.cn (X.N.)
[2] School of Metallurgical and Ecological Engineering, University of Science and Technology Beijing, Beijing 100083, China; a18811340254@163.com
* Correspondence: wgw676@163.com

Abstract: To solve the energy crisis and slow down the greenhouse effect, it is urgent to find alternative energy sources for the iron and steel production process. Hydrochar is an auxiliary fuel and the only renewable carbon source that could reduce the injection of bituminous coal into the blast furnace. Numerical simulation is an effective method of understanding the combustion performance in the lower part of the blast furnace. A 3D blowpipe-tuyere-raceway model was established using the computational fluid dynamics (CFD) method to study the effects on combustion performance between pulverized coal and hydrochar. The results showed that co-injection of anthracite and hydrochar has a better combustion performance than co-injection of anthracite and bituminous coal, with a more appropriate distribution of temperature, velocity, and gas phase. With the co-injection of hydrochar, the total burnout rate and anthracite burnout rate increased, respectively, by 6% and 2.1%, which is caused by the interaction mechanism between anthracite and hydrochar. As a result, hydrochar as an auxiliary fuel for blast furnace injection not only can achieve low-carbon production and cut down carbon emission but also benefit the combustion process of anthracite coal.

Keywords: hydrochar; co-injection; numerical simulation; the interaction mechanism

check for updates

Citation: Li, T.; Wang, G.; Zhou, H.; Ning, X.; Zhang, C. Numerical Simulation Study on the Effects of Co-Injection of Pulverized Coal and Hydrochar into the Blast Furnace. *Sustainability* **2022**, *14*, 4407. https://doi.org/10.3390/su14084407

Academic Editor: Rajesh Kumar Jyothi

Received: 6 March 2022
Accepted: 1 April 2022
Published: 7 April 2022

Publisher's Note: MDPI stays neutral with regard to jurisdictional claims in published maps and institutional affiliations.

Copyright: © 2022 by the authors. Licensee MDPI, Basel, Switzerland. This article is an open access article distributed under the terms and conditions of the Creative Commons Attribution (CC BY) license (https://creativecommons.org/licenses/by/4.0/).

1. Introduction

Iron and steel materials are the main structural materials in the 21st century. At present, the process of steel production is mainly divided into blast furnace ironmaking and non-blast furnace ironmaking. Although non-blast furnace ironmaking has developed rapidly in recent years, blast furnace ironmaking is still the main process of ironmaking [1]. The source of heat for blast furnace ironmaking mainly comes from the combustion of coke. However, with the exploitation of coke resources, the price of coke has risen, and it is urgent to find alternative energy sources for coke. The role of coke in blast furnace ironmaking is material column framework, heat source, reducing agent, and carburizing agent. The role of the column framework is irreplaceable, but other auxiliary fuels can be injected based on ensuring the column framework of coke to reduce the coke ratio, thereby reducing costs and reducing environmental pollution during the coking process [2,3]. Due to the distribution of resources in various countries, the injection of auxiliary fuels is also different, such as pulverized coal, natural gas, biochar, waste plastics, and oil [4,5]. Injecting pulverized coal is a very effective measure to reduce the coke ratio, which can reduce production costs and reduce energy consumption. At present, the average coal ratio in the furnace can reach 140 kg/tHM, and the highest coal ratio can reach 180 kg/tHM [6]. With the increase in the ratio of coal injected into the furnace, a large amount of unburned coal powder will be produced, which will affect the permeability of the charge and affect the forward flow of the blast furnace. Therefore, the injection of pulverized coal into the blast furnace has reached a certain limit [7,8]. Although the injection of pulverized coal into the blast furnace

can reduce pollution and cost to a certain extent, its effect is very limited compared with biomass fuel, because the amount of CO_2 released by the process of combustion is equal to the amount of CO_2 fixed in photosynthesis. Therefore, the injection of biomass fuel into the blast furnace has a more significant effect on energy saving and emission reduction than the injection of pulverized coal [9]. Biomass fuel, as a potential alternative energy source for fossil fuels and the only renewable carbon source, has a very wide range of application prospects and has received extensive attention from steel plants [10]. Combined with the distribution of China's biomass resources, the annual output of crop straw is about 740 million tons, which is equivalent to 200 million tons of standard coal [11]. Compared with fossil fuels, crop straw has lower sulfur, ash, and N content. The replacement of 1 ton of pulverized coal with crop straw can reduce the emission with 1.5 t CO_2 and 1 kg SO_2 [12]. Therefore, the application of hydrochar to the steel production process can not only improve the quality of the product but also achieve the purpose of low-carbon ironmaking. Since the current use of hydrochar is incineration, the utilization rate of maize straw is very low, only 33.3%, and direct incineration pollutes the environment more seriously [13]. To improve its utilization, researchers have found methods to purify and improve quality, such as pyrolysis and hydrothermal carbonization (HTC). Pyrolysis is a method that can increase the calorific value of biomass fuel that has been paid attention to by many scholars. Pyrolysis refers to the physical and chemical reaction carried out under high temperature and vacuum conditions. The purpose is to reduce the moisture and volatilization in biomass fuel [14]. However, the pyrolysis process is an energy-intensive process that consumes a lot of heat and emits a lot of air pollutants. However, hydrothermal carbonization (HTC) used biomass as the raw material, water as the liquid phase reaction medium, and at a certain temperature and pressure, the biomass is converted into hydrochar. A series of high-addition products is an efficient technology for recycling waste biomass. Compared with the pyrolysis process, the hydrothermal carbonization process (HTC) is an environment-friendly process with low energy consumption [15]. Therefore, it is paid attention by many researchers. Wang et al. and other researchers have found through experimental studies that the hydrotchar after HTC treatment, which is treated at 280 °C, is very similar to pulverized coal in proximate analysis and ultimate analysis or H/C, O/C, and calorific value [16]. The reactivity of hydrochar after 60 min is even better than that of bituminous coal [14]. In addition, different researchers have also proved that the hydrochar obtained after HTC treatment has better energy density, solubility, and lower alkali metal content, so it is beneficial to blast furnace ironmaking [17–19]. Through experimental studies, Liu et al. showed that the time and temperature of hydrothermal carbonization are important factors affecting the quality of hydrochar. Wang et al. used corn stalks as raw materials and set different hydrothermal carbonization times and temperatures to prove that the hydrochar obtained after hydrothermal carbonization at 280 °C for 60 min has better calorific value and reactivity than pulverized coal [16,20]. In summary, hydrochar is a very clean renewable energy, and the steel production process is a big consumer of CO_2 emissions with energy consumption. Therefore, using hydrochar for blast furnace injection can alleviate the energy crisis and greenhouse emissions.

It is very difficult to observe the details of physical and chemical reactions occurring inside the blast furnace in actual production. With the development of computers and mathematical models, it is possible to establish mathematical models and use computational fluid dynamics (CFD) to simulate the reactions occurring inside the blast furnace, like gas composition distribution, velocity field, and temperature field. Different researchers have long-established mathematical models to simulate the combustion performance in the lower part of the blast furnace from different scales. In 1980, Takeda and Lockwood et al. established an early two-dimensional pulverized coal injection model to study the tuyere + raceway area and the combustion performance of pulverized coal in the coke bed [21,22]. According to the actual blast furnace production situation, a three-dimensional mathematical model is needed. Du et al. established a three-dimensional mathematical model of the blowpipe and the tuyere and studied the combustion perfor-

mance of the pulverized coal in the blowpipe and the tuyere under different operating conditions. To have a more comprehensive understanding of the combustion performance of pulverized coal in the raceway under three-dimensional conditions, Shen et al. established a three-dimensional mathematical model of blowpipe + tuyere + raceway to understand the combustion performance of blast furnace pulverized coal more comprehensively. The combustion includes the combustion of pulverized coal and coke. Moreover, Shen and others have further improved the three-dimensional mathematical model of the blast furnace by establishing a three-dimensional mathematical model of the combustion of pulverized coal and coke [23–25].

The blast furnace is like a black box; it is difficult to directly observe the specific combustion phenomenon in the tuyere and raceway. Previous studies have proved that the establishment of mathematical models can provide a more economical, safer, and effective method for understanding the complex reactions occurring inside the blast furnace. Moreover, studies have proved that there is a synergistic effect between hydrochar combustion and pulverized coal combustion [26], but few papers have detailed the specific mechanism and effects on combustion performance of co-injection of pulverized coal and hydrochar, in order to solve the energy crisis, reduce the pollution caused by blast furnace ironmaking to the environment, and help realize low carbon ironmaking as soon as possible. In this paper, by establishing a three-dimensional mathematical model (blowpipe + tuyere + raceway), selecting the hydrochar treated under the condition of 280 °C for 60 min as the experimental material, and using the actual operating parameters of China AnSteel as the boundary conditions, the effects of combustion performance on co-injection of pulverized coal and hydrochar are further studied, which can provide theoretical guidance for the actual blast furnace co-injection of pulverized coal and hydrochar.

2. Model Description

2.1. Model Simplification

A variety of physical and chemical reaction processes occurred in the raceway. The main reaction processes include (a) gas-phase flow; (b) turbulent flow of pulverized coal particles in gas-phase flow; (c) combustion of pulverized coal; (d)combustion (evaporation of water, devolatilization, combustion of fixed carbon and volatile); (d) heat transfer between gas and fuel particle. To reduce the burden of calculation, the assumptions are as follows: (1) the coal particles are defined as spheres, regardless of the collision, and the effect of unburned coal on the combustion system will be ignored; (2) the operation status of the blast furnace is stable, so the size of the raceway is fixed; (3) the composition of hydrochar is very similar to that of coal powder in previous studies, so hydrochar is regarded as a coal-like material injected into the blast furnace [16]; (4) the coke combustion reaction is more complicated, this model excludes the phenomenon of coke combustion, and the combustion behavior of pulverized coal and hydrochar is only considered; (5) to simulate the physical and chemical reaction of pulverized coal and hydrochar from the lance to the raceway zone more precisely. The process, according to the anatomical diagram of the lower part of the AnSeel blast furnace Figure 1, is to simplify the blowpipe, coal lance, tuyere, and raceway into a whole cavity; its geometric model and geometric parameters are listed in Figure 2.

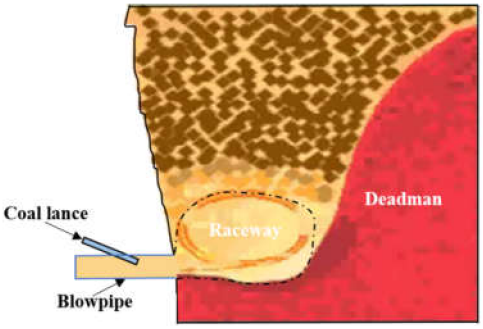


Figure 1. Structure of lower part of blast furnace.

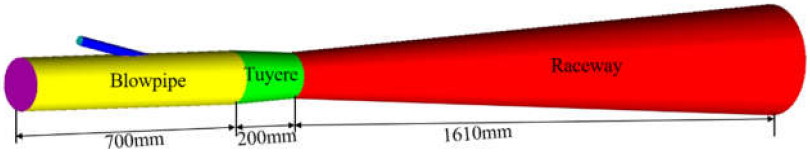


Figure 2. Geometry model and parameters.

2.2. Basic Governing Equations

2.2.1. Continuous Phase

Due to the full development of the fluid flow in the tuyere, the gas phase is transferred to the continuous phase, and the high-velocity gas flow (carrier gas and blast) is described through the 3D-steady state, Reynolds-averaged Navier–Stokes equations, and k-ε turbulence model equations. To obtain these variables such as velocity, pressure, and mass fraction of the gas phase, the above equations will be solved. The governing equations are listed in Table 1 [27,28]:

Table 1. Governing equations of the continuous phase.

Momentum	$\nabla \cdot (\rho UU) - \nabla \cdot \left[(\mu + \mu_t)\left(\nabla U + (\nabla U)^T\right)\right] = -\nabla\left(p + \frac{2}{3}\rho k\right) + \sum_{n_p} f_D$
Energy gas	$\nabla \cdot \left[\rho UH - \left(\frac{\lambda}{C_P} + \frac{\mu_t}{\sigma_H}\right)\right] = \sum_{n_p} q$
Species	$\nabla \cdot \left[\rho UY_i - \left(\frac{\lambda}{\Gamma_i} + \frac{\mu_i}{\sigma_{Yi}}\right)\right] = W_i$
Turbulent kinetic energy	$\nabla \cdot \left[\rho Uk - \left(\mu + \frac{\mu_t}{\sigma_k}\right)\nabla k\right] = p_k - \rho\varepsilon$
Turbulent dissipation rate	$\nabla \cdot \left[\rho U\varepsilon - \left(\mu + \frac{\mu_t}{\sigma_\varepsilon}\right)\nabla \varepsilon\right] = \frac{\varepsilon}{k}(C_1 p_k - C_{2\rho\varepsilon})$

2.2.2. Discrete Phase

In this model, pulverized coal particles and hydrochar particles are regarded as discrete phases, the Lagrangian method is combined with Newton's second law of motion, and the random trajectory model is used to solve to track the trajectory of the particles. The heat transfer between the fuel particles and between the fuel particles and the gas phase is simulated through convex heat transfer, latent heat transfer with mass transfer, and radiative heat transfer [29,30]. The governing equations are shown in Table 2.

Table 2. Governing equations for the discrete phase.

Mass	$\frac{dm_p}{dt} = \dot{m}$
Momentum	$m_p \frac{du_p}{dt} = -f_D$ $-f_D = \frac{1}{8}\pi d_p^2 \rho C_D \lvert U - U_P \rvert (U - U_P)$
Energy	$m_p C_p \frac{dT_p}{dt} = h_{i,\mathrm{conv}} A_p (T_g - T_p) + \sum \frac{dm_p}{dt} H_{\mathrm{reac}} + A_p \varepsilon_p \sigma_B \left(T_{\mathrm{rad}}^4 - T_p^4\right)$

The combustion of pulverized coal and hydrochar in the blast furnace is a multi-step reaction, which specifically includes: (1) the preheating of pulverized coal and hydrochar; (2) the devolatilization process of pulverized coal and hydrochar; (3) the combustion of volatiles in pulverized coal and hydrochar, combustion and gasification of residual carbon in pulverized coal and hydrochar particles. In this model, the devolatilization process is treated in the two-competing-reactions model [31], the so-called two-competing-reactions model refers to two devolatilization processes for pulverized coal and hydrochar at high and low temperatures with two different devolatilization rates as follows in Equation (1):

$$\begin{array}{c} High-temperature: \alpha_1 V_1 M_1 + (1-\alpha_1) Char_1 \\ Low-temperature: \alpha_2 V_2 M_2 + (1-\alpha_2) Char_2 \end{array} \quad (1)$$

where α_1 and α_2 are the reaction rate constants in the Arrhenius formula, α_1 = VM (daf); $\alpha_2 = 1.25\alpha_1 + 0.92\alpha_1$.

In industrial problems, the volatile matter is usually considered a mixture of various fuel gas. The chemical reaction of volatile matter and residual carbon combustion and its kinetic parameters are shown in Table 3 [32]:

$$VM + O_2 = CO_2 + H_2O + N_2$$

$$Char + 0.5O_2 = CO$$

$$Char + CO_2 = 2CO$$

$$Char + H_2O = CO + H_2$$

Table 3. Reaction rates for the coal particle.

Reaction	Reaction Kinetics
$VM + O_2 = CO_2 + H_2O + N_2$	$A = 2.1 \times 10^{11}\ s^{-1}$ $E = 2.03 \times 10^{8}\ J{\cdot}mol^{-1}$
$Char + 0.5O_2 = CO$	$A = 2.1 \times 10^{11}\ s^{-1}$ $E = 2.033 + 08\ J{\cdot}mol^{-1}$ $\beta = 0.68$
$Char + CO_2 = 2CO$	$A = 6.783 + 4\ s^{-1}$ $E = 3.63 \times 10^{8}\ J{\cdot}mol^{-1}$ $\beta = 0.68$
$Char + H_2O = CO + H_2$	$A = 8.55 \times 10^{4}\ s^{-1}$ $E = 3.4 \times 10^{8}\ J{\cdot}mol^{-1}$

2.3. Operation Conditions

The geometric model is established according to the actual size of the China AnSteel 3200 m^3 blast furnace. The geometric model is shown in Figure 2. The diameter of the blowpipe is 140 mm, the depth of the raceway is 1610 mm, and the outlet of the coal lance is located at the center line of the raceway, the inclined angle is 12°. The main operating parameters are shown in Table 4. According to the actual production situation, the diameter of the pulverized coal particles is 74 μm; this paper designs two cases to study the effects of the co-injection of pulverized coal/hydrochar: (a) 45% Anthracite + 55% Bituminous (Coal); (b) 45% Anthracite + 55% Hydrochar (HC). The hydrochar used in this article is a sample of maize straw after HTC treatment at 280 °C and 60 min [16]. The proximate analysis, ultimate analysis, and calorific value of hydrochar and coal are shown in Table 5.

Table 4. Operating conditions and parameters.

Operating Conditions	Values
Tuyere number of BF	32
Utilization (t/(m^3·d))	2.41
Blast flow rate (m^3/min)	5192
Pressure (kPa)	385
Coal ratio (kg/tHM)	147
Blast temperature (K)	1473
Conveying gas temperature (K)	296
Coal temperature (K)	333
Conveying gas flow rate (m^3/min)	1800
Conveying gas of pulverized coal	N_2

Table 5. Properties of coal and hydrochar.

Sample	Proximate Analysis (wt, %)			Ultimate Analysis (wt, %)					HHV(MJ/kg)
	FC_d [a]	A_d	V_d	C_{daf}	H_{daf}	O_{daf} [a]	N_{daf}	S_{daf}	
Anthracite	79.48	12.2	8.32	82.06	3.26	0.68	1.18	0.62	36.2
Bituminous	58.71	6.84	34.45	65.92	4.98	15.88	0.71	0.31	29.7
Hydrochar	47.28	2.07	50.65	65.43	4.80	16.22	1.22	0.12	28.7

Note: [a] Calculated by difference. FC, fixed carbon; A, ash; V, volatile matter; d, dry basis; daf, dry ash-free.

3. Results and Discussion

To ensure the accuracy of simulation results, the single variable—the type of fuel injection (hydrochar/coal)—was changed under the basic condition of the operating parameters, geometric model, and mathematical model, in order to study the effects of co-injection of pulverized coal and hydrochar. The simulation results and analysis will be discussed, to provide theoretical guidance for actual production.

3.1. Model Validation

The validity of the model has been studied by several researchers. Predecessors have used computational fluid dynamics (CFD) to carry out a large number of numerical simulation studies on co-injection pulverized coal [33,34]. Shen et al. proved the validity of the model and calculation results [24,35]. In addition, Zhang et al. also proved the accuracy and validity of the calculation results of the injection of hydrochar into the blast furnace through numerical simulations [36,37]. Therefore, by changing the type of fuel injection (coal/hydrochar) a single variable changed, which fully proves the validation of the model. Due to that the blast furnace tuyeres are symmetrical in geometry, the center symmetry plane was selected to study the gas flow, gas-phase distribution, and temperature distribution under the case of basic conditions and the case of co-injection pulverized coal and hydrochar into the blast furnace.

3.2. Velocity Distribution

Figure 3 is the contour of the velocity of the continuous phase (hot blast, carrier gas, volatile) on the central symmetry plane of the model. Figure 4 is the velocity trend along the fuel plume. From Figures 3 and 4, it can be seen that the velocity of the carrier gas in coal lance is 15 m/s, and the velocity of the gas phase in the blowpipe is 210 m/s, which is the velocity of the hot blast. In both cases, the maximum velocity reached the raceway-top area, and the value is 311 m/s (HC) and 306 m/s (Coal). Combining the numerical simulation results and the size of the tuyere, it can be seen that this is due to the entry of carrier gas and fuel particle in the coal lance when the hot blast enters the tuyere. As a result, fuel particles make the gas mass flow rate here larger, and the diameter of the inlet of tuyere is slightly smaller than the diameter of the inlet of the blowpipe. Therefore, when the gas passes through the tuyere, there will be an acceleration process to reach the maximum velocity at the raceway-top area. When the gas enters the raceway, as

the diameter of the raceway gradually increases, the velocity of the gas phase gradually decreases. The trend of the velocity contour of the gas phase in the two cases is almost the same. The slight difference is that the maximum velocity area is different in the two cases. The maximum velocity area in the case of pulverized coal injection individual is only at the tuyere. When the maximum velocity is reached at the tuyere under the co-injection of hydrochar, the maximum velocity area still exists in the raceway. This is caused by a large amount of CO_2 is generated in the high-velocity area when co-injecting coal and hydrochar. However, the amount of CO_2 produced here is relatively smaller in the case of pulverized coal injection, and the temperature of the area in the case of co-injection of hydrochar is higher (Figure 5), Therefore, a large amount of CO_2 heated and expanded increased the velocity in this area. After monitoring, it was found that the mass flow rate at the outlet of the pulverized coal was 1.77 kg/s, and the mass flow rate at the outlet when hydrochar was co-injected was 2.04 kg/s. In one word, the larger gas flow rate and more volatile matter formed the high-velocity zone still exist in the upper part of the raceway when the hydrochar is co-injected.

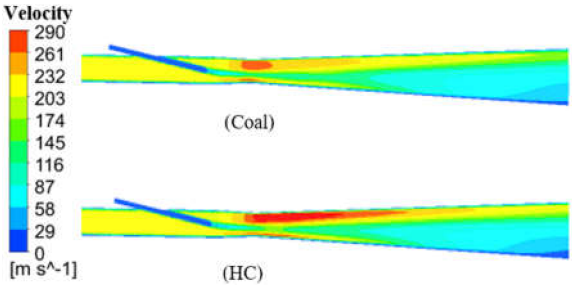


Figure 3. Contour of the velocity at the symmetric plane (Coal 45% Anthracite + 55% Bituminous; HC: 45% Anthracite + 55% Hydrochar).

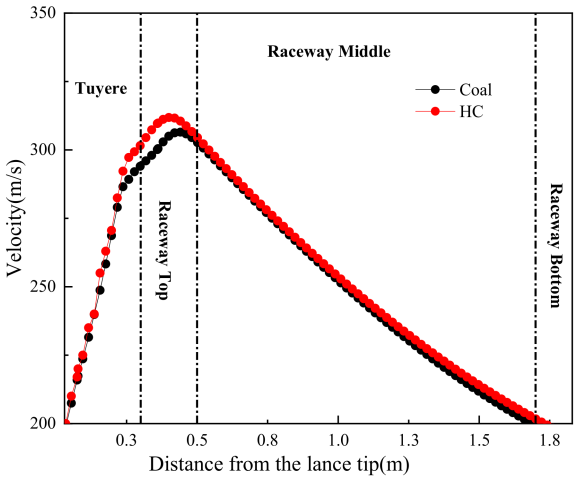


Figure 4. Velocity changed trend along the fuel plume (Coal 45% Anthracite + 55% Bituminous; HC: 45% Anthracite + 55% Hydrochar).

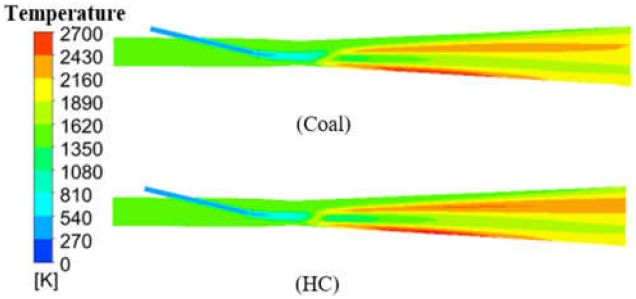


Figure 5. Contour of the temperature at the symmetric plane (Coal 45% Anthracite + 55% Bituminous; HC: 45% Anthracite + 55% Hydrochar).

3.3. Temperature and Gas-Phase Distribution

Figure 5 shows the contour of the temperature at the central symmetry plane in both cases. It can be seen from Figure 5 that the temperature did not rise until the gas phase and fuel particles entered the raceway, and there is a low-temperature area in the tuyere. As shown in Figure 6, in this area, in the meantime, O_2 was also less consumed, which revealed that the fuel particles are not almost combusted in the tuyere (Figure 7), and the heat was absorbed by devolatilization to form a low-temperature area. As the fuel particles entered the raceway, the massive combustion of volatile and residual carbon caused the temperature to rise quickly. When pulverized coal was injected individually, the maximum temperature in the raceway could reach 2638 K, and the maximum temperature in the tuyere raceway could reach 2703 K when the hydrochar was co-injected (Figure 8). The reason for the highest temperature is that hydrochar characterizes a higher volatile content and higher calorific value. Otherwise, combined with the simulation results (Figure 9), hydrochar devolatilized earlier and combusted earlier, thereby promoting the combustion of residual carbon. In both cases, the high-temperature zone in the raceway is distributed along the outer side of the coal plume. This was caused by a higher surface area/mass ratio and a higher O_2 concentration on the outside of the coal plume and the residual carbon can be consumed more fully.

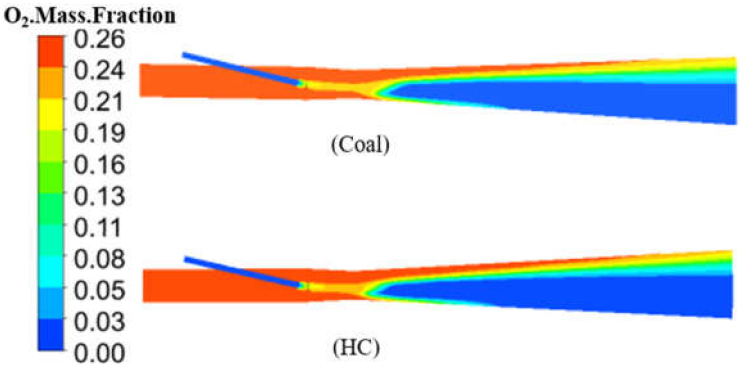


Figure 6. Contour of the of O_2 at the symmetric plane (Coal 45% Anthracite + 55% Bituminous; HC: 45% Anthracite + 55% Hydrochar).

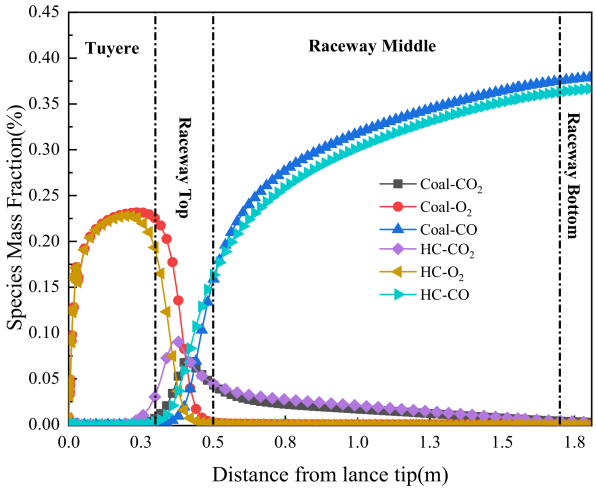


Figure 7. Gas-phase Mass fraction of two cases along the fuel plume (Coal 45% Anthracite + 55% Bituminous; HC: 45% Anthracite + 55% Hydrochar).

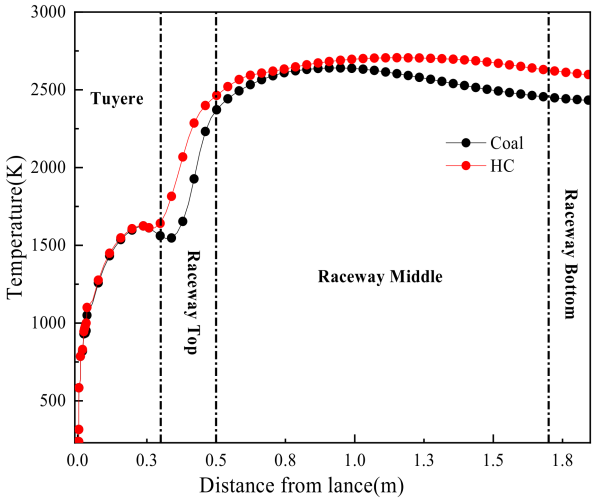


Figure 8. Temperature changed trend along the fuel plume (Coal 45% Anthracite + 55% Bituminous; HC: 45% Anthracite + 55% Hydrochar).

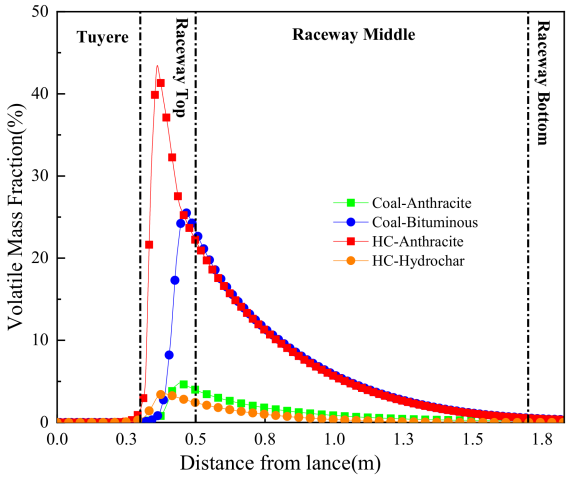


Figure 9. Mass fraction of volatile along the fuel plume (Coal 45% Anthracite + 55% Bituminous; HC: 45% Anthracite + 55% Hydrochar).

Figures 6 and 10 are the contours of the mass fractions of O_2, CO_2, and CO, which are distributed at the central symmetry plane in the two cases, respectively. Figure 8 shows the changed trend of the mass fractions of O_2, CO_2, CO, and volatile mass along the fuel plume. Figures 7 and 9 can be divided into four parts: tuyere, raceway-top, raceway-middle, raceway-bottom. It can be seen from Figure 6 that the O_2 concentration in the blowpipe was maintained at 26% in both cases. When the hot blast reached the coal lance, the coal lance had a certain insertion angle, so that the O_2 concentration at the outlet of the coal lance was 0. As the hot blast gradually moved away from the exit of the coal lance, O_2 re-aggregated. In addition, due to the addition of fuel particles and carrier gas and the generation of volatiles, the O_2 concentration was diluted, so there was a trend of O_2 concentration increasing from 0 in Figure 7 (tuyere area). When the hot blast passed through the inlet of the raceway (Figure 7, raceway-top), the O_2 concentration slowly decreased. Combined with Figure 7 (raceway-top), it can be seen that when the O_2 concentration dropped significantly, CO_2 and CO began to be produced. The simulation results (Figure 7, raceway-top) showed that volatile matter and residual carbon began to consume O_2 and combust, and in the meantime, the residual carbon was vaporized. In addition, it can be seen from Figure 10b that there is no big difference in the concentration field of CO in the two cases, and the changing trend is the same (Figure 10b). In the case of co-injection of hydrochar, (Figure 10a raceway-top), there is a CO_2 enriched area on the outside of the particle plume. This was caused by the more volatile content of the hydrochar and more opportunities to react with O_2 on the outside of the fuel plume; there is also a gradual area of O_2 concentration on the outside (Figure 4). As the fuel particles continued to enter the raceway and began to combust and consume O_2, the O_2 concentration suddenly dropped until it disappeared (Figure 7, raceway-middle + raceway-bottom). Therefore, the area of the particle tracks in the raceway is the O_2-depleted area. The mass fraction of O_2 was 0 within the range of $\geq$0.5 m from the exit of the coal lance, so the combustion of volatile matter and residual carbon was completed fully at the bottom part of the raceway (Figure 9 raceway-top). As the fuel particles entered the middle part of the raceway, it can be seen from Figure 6 that in the O_2-depleted zone, the concentration of CO_2 began to decrease, while the concentration of CO rose suddenly. This was caused as the devolatilization of fuel particles progressed; residual carbon was exposed gradually and interacted with CO_2, causing the concentration of CO to rise (Figure 7, raceway-middle). As the residual carbon gasification reaction progressed, the mass fraction of CO_2 and residual carbon gradually decreased, so that the reaction rate and the rate of CO generation slowed down (Figure 7, bottom), until the CO_2 disappeared at the exit of the raceway, and the CO concentration reached the maximum value (Figure 7, raceway-bottom). It can be seen from the simulation results that more CO is produced when the co-injection of hydrochar is due to the production of more CO_2. A higher concentration of CO is beneficial to increasing the utilization rate of fuel gas.

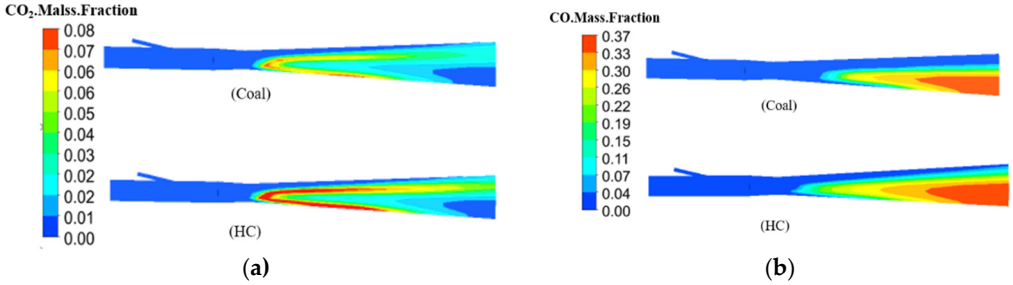


Figure 10. Contour of the of CO_2 (**a**) and CO (**b**) at the symmetric plane (Coal 45% Anthracite + 55% Bituminous; HC: 45% Anthracite + 55% Hydrochar).

3.4. Burnout Rate

The burnout rate is an important indicator to evaluate the degree of fuel combustion performance, which presented the loss of mass resulted from the combustion of volatile matter and the combustion and gasification of residual char [34]. A large number of un-

burned fuel particles entering the coke bed will seriously affect its permeability. Therefore, it is necessary to study the burnout rate of fuel particles. The calculation formula for burnout rate is shown in the formula [24]:

$$Burnout = \frac{1 - \frac{X_{a,0}}{X_a}}{1 - X_{a,0}} \times 100\% \quad (2)$$

where $X_{a,0}$ is the original ash mass fraction of solid particles and X_a is the mass fraction of ash.

Figure 11 shows the variation trend of the individual burnout rate and the total burnout rate of a single fuel particle along the centerline of the tuyere and raceway in the two cases. It can be seen from Figure 11 that there was no significant change in the burn-out rate of fuel particles in the tuyere. The devolatilization process was mainly carried out in this area. From the simulation results of Figure 7, it can be seen that no CO and CO_2 were produced in this area. As a result, there is no large amount of combustion phenomenon. The burnout rate suddenly rose at the top part of the raceway. This is due to the gradual exposure of residual carbon particles with the progress of particle devolatilization so that they are in contact with O_2 and CO_2. This area mainly produces volatile matter and combustion and gasification of residual carbon. In the middle part of the raceway, the burnout rate continued to rise but the trend became slower. It can be seen from the simulation results (Figure 7) that this part of the burnout rate rise is caused by the gasification of residual carbon, and the slower trend is due to the gasification of residual carbon in the fuel particles, the mass fraction of residual carbon, and a CO_2 decrease, which slow the reaction rate. The gas-phase mass fraction of CO_2 and O_2 at the outlet of the raceway disappeared, and the burnout rate was reached and maintained at maximum value. The simulation results show that the fuel particles in this range were fully gasified, so the burnout rate remained at maximum value.

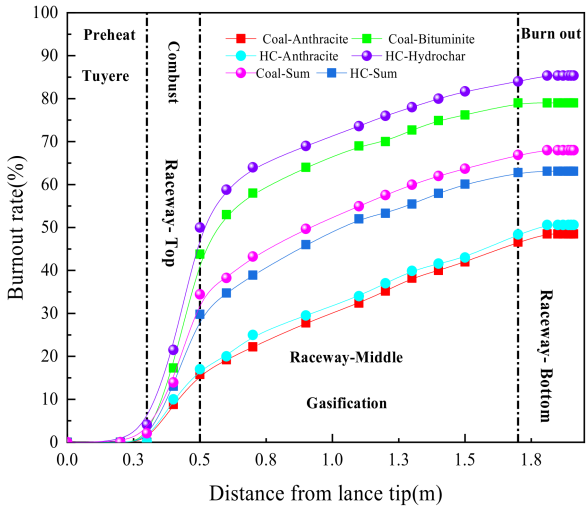


Figure 11. Burnout rate changed trend along the fuel plume. (Coal 45% Anthracite + 55% Bituminous; HC: 45% Anthracite + 55% Hydrochar.)

Comparing the burnout rate in the two cases, it can be found that both the individual burnout rate and the total burnout rate in the case of co-injection of hydrochar are higher than the burnout rate in the case of pulverized coal injection. The highest burn-out rates of anthracite and bituminous coal in the case of pulverized coal injection individuals can reach 48.5% and 79%. In the case of co-injection of hydrochar, the highest burn-out rates of anthracite and hydrochar can reach 50.6% and 85.37%. The total burnout rate in the two cases is 73% (Coal) and 79% (HC), respectively. It can be seen from the simulation results (Figure 9) that, on the one hand, because hydrochar has more volatile content and higher calorific value than bituminous coal, it is devolatilized and combusts earlier and releases

more heat. This part of heat will promote the devolatilization of anthracite and preheat the anthracite particle better. On the other hand, the hydrochar releases more volatile matter, its combustion will generate more CO_2, and it will promote the gasification of the residual carbon.

4. Conclusions

A three-dimensional model was established to study the flow field, temperature field, gas-phase distribution, and burnout rate. The effect on co-injection hydrochar and coal were studied, respectively. The main conclusions are as follows:

(1) According to the simulation of the two cases, there is no obvious difference in the velocity field. The maximum velocity reached in both cases is, respectively, 311 m/s and 306 m/s; co-injection of hydrochar with a higher velocity and with a wider high-velocity area in the raceway along the outside of the fuel plume. The gas permeability of the coke bed and the development of the central gas will benefit from a higher flow mass rate.

(2) A higher maximum temperature (65 K) and a wider high-temperature area in the tuyere occurred, due to the co-injection of hydrochar with a higher volatile content and higher calorific value, which can accelerate the process of coal combustion.

(3) An appropriate gas phase distribution plays a key role in smelting and burnout rate. With the co-injection of hydrochar, a higher mass fraction of CO_2 and CO was produced by gasification and combustion of residual carbon and volatile matter, which both have a positive effect on increasing the burn-out rate and improving the reduction degree of iron ore and the utilization rate of fuel gas.

(4) In addition, a higher individual burnout rate of anthracite (2.1%) and total burnout rate (6%) was derived due to the effects on co-injection of hydrochar and pulverized coal, which can promote the goal of a lower fuel ratio and cost of production. In a word, co-injection of hydrochar has a better overall combustion performance; furthermore, the photosynthesis of the raw material combined with hydrochar is more conducive to achieving the goal of reducing cost and slowing down the greenhouse effect.

Author Contributions: Investigation, C.Z.; Validation, X.N.; Writing—original draft, T.L.; Writing—review & editing, G.W. and H.Z. All authors have read and agreed to the published version of the manuscript.

Funding: This research was funded by National Natural Science Foundation of China: No. 52074029 and No.52174295.

Institutional Review Board Statement: Not applicable.

Informed Consent Statement: Not applicable.

Data Availability Statement: Not applicable.

Conflicts of Interest: The authors declare no conflict of interest.

References

1. Shen, Y.; Yu, A.; Zulli, P. CFD Modelling and Analysis of Pulverized Coal Injection in Blast Furnace: An Overview. *Steel Res. Int.* **2011**, *82*, 532–542. [CrossRef]
2. Wang, H.Y.; Zhang, J.L.; Liu, S.Y. Feasibility research of brown coal injection for blast furnace. *J. IronsSteel* **2006**, *1*, 10–14.
3. John, G.M.; John, S.T.; Harold, R. Toward an understanding of coal combustion in blast furnace tuyere injection. *Fuel* **2005**, *84*, 1229–1237.
4. Hu, Z.W.; Zhang, J.L.; Zuo, H.B.; Li, J.; Liu, Z.J.; Yang, T.J. Preparation and properties of biomass char for ironmaking. *Chin. J. Eng.* **2012**, *34*, 998–1005.
5. Gao, L.; Zhang, J.H.; He, Z.J.; Pang, Q.H.; Zhan, W.L. Study on experimental simulation of the co-injection of waste plastics and pulverized coal into rotary kiln. *Sint. Pelletizing* **2015**, *40*, 38–43. [CrossRef]
6. Wang, W.X. Review on the technology of iron-making in China in 2019. In Proceedings of the Annual Meeting of China Metal Society, Tianshui, China, 5 July 2019. [CrossRef]

7. Suzuki, T.; Smoot, L.D.; Fletcher, T.H.; Smith, P. Prediction of High-Intensity Pulverized Coal Combustion. *Combust. Sci. Technol.* **1986**, *45*, 167–183. [CrossRef]
8. Nogami, H.; Miura, T.; Furukawa, T. Simulation of Transport Phenomena around Raceway Zone in the Lower Part of Blast Furnace. *Tetsu-to-Hagane* **1992**, *78*, 1222–1229. [CrossRef]
9. Abbasi, T.; Abbasi, S. Biomass energy and the environmental impacts associated with its production and utilization. *Renew. Sustain. Energy Rev.* **2010**, *14*, 919–937. [CrossRef]
10. Suopajärvi, H.; Kemppainen, A.; Haapakangas, J.; Fabritius, T. Extensive review of the opportunities to use biomass-based fuels in iron and steelmaking processes. *J. Clean. Prod.* **2017**, *148*, 709–734. [CrossRef]
11. Geng, W.W.; Zuo, H.B.; Wang, G.W. Application of biomass in ironmaking raw materials research. In Proceedings of the Annual Conference of Ironmaking Scholars, Zhengzhou, China, 13 May 2014; pp. 312–316.
12. Chen, D.F.; Hu, X.Y.; Li, X.J. Biomass resource's application in iron and steel enterprises of China. *Res. Iron. Steel* **2015**, *43*, 60–62.
13. Xiong, W.; Wang, G.Q.; Zhou, S.X. Comparison of energy consumption and environmental impact of replacement of coal with straw injection into blast furnace. *Environ. Sci. Technol.* **2013**, *36*, 137–140.
14. Wang, G.; Zhang, J.; Zhang, G.; Ning, X.; Li, X.; Liu, Z.; Guo, J. Experimental and kinetic studies on co-gasification of petroleum coke and biomass char blends. *Energy* **2017**, *131*, 27–40. [CrossRef]
15. Gao, P.; Zhou, Y.; Meng, F.; Zhang, Y.; Liu, Z.; Zhang, W.; Xue, G. Preparation and characterization of hydrochar from waste eucalyptus bark by hydrothermal carbonization. *Energy* **2016**, *97*, 238–245. [CrossRef]
16. Wang, G.; Zhang, J.; Lee, J.-Y.; Mao, X.; Ye, L.; Xu, W.; Ning, X.; Zhang, N.; Teng, H.; Wang, C. Hydrothermal carbonization of maize straw for hydrochar production and its injection for blast furnace. *Appl. Energy* **2020**, *266*, 114818. [CrossRef]
17. Mäkelä, M.; Volpe, M.; Volpe, R.; Fiori, L.; Dahl, O. Spatially resolved spectral determination of polysaccharides in hydrothermally carbonized biomass. *Green Chem.* **2018**, *20*, 1114–1120. [CrossRef]
18. Lokahita, B.; Aziz, M.; Yoshikawa, K.; Takahashi, F. Energy and resource recovery from Tetra Pak waste using hydrothermal treatment. *Appl. Energy* **2017**, *207*, 107–113. [CrossRef]
19. Lu, L.; Namioka, T.; Yoshikawa, K. Effects of hydrothermal treatment on characteristics and combustion behaviors of municipal solid wastes. *Appl. Energy* **2011**, *88*, 3659–3664. [CrossRef]
20. Liu, F.Y.; Yu, R.D.; Ji, X.D. Hydrothermal carbonization of holocellulose into hydrochar: Structual, chemical characteristics, and combustion behavior. *Bioresour. Technol.* **2018**, *263*, 508–516. [CrossRef]
21. Takeda, K.; Lockwood, F.C. Integrated mathematical model of pulverised coal combustion in a blast furnace. *ISIJ Int.* **1997**, *37*, 432–440. [CrossRef]
22. Shen, Y.S.; Guo, B.Y.; Yu, A.B. Three-Dimensional Modelling of Coal Combustion in Blast Furnace. *ISIJ Int.* **2008**, *48*, 777–786. [CrossRef]
23. Du, S.-W.; Chen, W.-H.; Lucas, J. Performances of pulverized coal injection in blowpipe and tuyere at various operational conditions. *Energy Convers. Manag.* **2007**, *48*, 2069–2076. [CrossRef]
24. Shen, Y.; Maldonado, D.; Guo, B.Y.; Yu, A.; Austin, P.; Zulli, P. Computational Fluid Dynamics Study of Pulverized Coal Combustion in Blast Furnace Raceway. *Ind. Eng. Chem. Res.* **2009**, *48*, 10314–10323. [CrossRef]
25. Maldonado, D.; Austin, P.R.; Zulli, P. *Modeling Coal Combustion Behavior in an Ironmaking Blast Furnace Raceway: Model Development and Applications*; AISTech: Barcelona, Spain, 2009; p. 50.
26. Wang, Q.; Wang, E.L.; Oguga, P.C. Numerical simulation of the synergistic effect of combustion for the hydrochar /coal blends in a blast furnace. *Energy* **2022**, 238. [CrossRef]
27. Launder, B.E.; Spalding, D.B. The numerical computation of turbulent flows. *Comput. Meth Appl. Mech. Eng.* **1974**, *3*, 269–289. [CrossRef]
28. Silaen, A.; Wang, T. Effect of turbulence and devolatilization models on coal gasification simulation in an entrained-flow gasifier. *Int. J. Heat Mass Transf.* **2010**, *53*, 2074–2091. [CrossRef]
29. Wijayanta, A.T.; Alam, S.; Nakaso, K.; Fukai, J.; Kunitomo, K.; Shimizu, M. Numerical Study on Pulverized Biochar Injection in Blast Furnace. *ISIJ Int.* **2014**, *54*, 1521–1529. [CrossRef]
30. Yu, A.; Xu, B. Particle-scale modelling of gas–solid flow in fluidisation. *J. Chem. Technol. Biotechnol.* **2003**, *78*, 111–121. [CrossRef]
31. Nogami, H.; Yamaoka, H.; Takatani, K. Raceway design for the innovative blast furnace. *ISIJ Int.* **2004**, *44*, 2150–2158. [CrossRef]
32. Ubhayakar, S.K.; Stickler, D.B.; Von Rosenberg, C.W.; Gannon, R.E. Rapid devolatilization of pulverized coal in hot combustion gases. *Symp. (International) Combust.* **1977**, *16*, 427–436. [CrossRef]
33. Du, S.W.; Chen, W.H. Numerical prediction and practical improvement of pulverized coal combustion in blast Furnace. *International Commun. Heat Mass Transf.* **2006**, *33*, 327–334. [CrossRef]
34. Li, Y.; Zhang, X.; Zhang, J.; Zhou, J.; Yan, H. Numerical simulation and optimization of pulverized coal injection with enriched oxygen into blast furnace. *Appl. Therm. Eng.* **2014**, *67*, 72–79. [CrossRef]
35. Hu, Z.J.; Liu, Y.R.; Xu, H. Co-combustion of semi-coke and coal in an industry ironmaking blast furnace: Lab experiments, model study and plant tests. *Fuel Process Technol.* **2019**, *196*, 1–13. [CrossRef]
36. Liu, Y.; Shen, Y. Combined Experimental and Numerical Study of Charcoal Injection in a Blast Furnace: Effect of Biomass Pretreatment. *Energy Fuels* **2020**, *34*, 827–841. [CrossRef]
37. Zhang, C.; Wang, G.; Ning, X.; Zhang, J.; Wang, C. Numerical simulation of combustion behaviors of hydrochar derived from low-rank coal in the raceway of blast furnace. *Fuel* **2020**, *278*, 118267. [CrossRef]